Journal of Radioanalytical and Nuclear Chemistry, Articles, Vol. 112, No. 1 (1987) 57–64

2-D RECONSTRUCTION OF ELEMENTAL DISTRIBUTION WITHIN A SAMPLE USING NEUTRON CAPTURE PROMPT GAMMA-RAYS

N. M. SPYROU KUSMINARTO, G. E. NICOLAOU

Department of Physics, University of Surrey, Guildford, Surrey GU2 5XH (UK)

(Received December 12, 1986)

The technique of emission tomography employing neutron capture prompt gamma-rays is described. Experiments have been carried out to demonstrate this technique employing a high flux reactor neutron beam using an HPGe detector and a scanning system which incorporates a BBC microcomputer for control, data acquisition, image reconstruction and display. Neutron tomography of the same object was also performed in order to correct the emission tomography results for the neutron flux depression within the sample. The images produced represent the intensity of the induced gamma-ray of interest, and hence the concentration of the isotope of interest.

Introduction

Instrumental Neutron Activation Analysis (INAA) has been extensively used and well established as a method to determine the concentration of elements in a variety of samples.

In other areas, reconstructive tomography has also been widely used to examine the internal structure and composition of objects, employing X-rays in transmission mode and gamma-rays in both emission and transmission modes. Combination of the methods of INAA and tomography should produce an excellent method for the non-destructive mapping of the elements present in an object.

A method of emission tomography based on the detection of delayed gamma-rays emitted by the object following neutron irradiation has been used successfully to examine simulated reactor fuel /1/ and the elemental distribution within a bone sample /2/. In the case when very short-lived isotopes are produced, this technique is not suitable because of the time required for data acquisition. Therefore, a tomographic technique based on the detection of prompt gamma-rays emitted by the object during neutron irradiation was investigated /3/.

The two major problems with neutron capture prompt gamma-ray emission tomography are the neutron flux depression which occurs when the neutron beam traverses the object and the attenuation of photons within the object itself. The former case can be overcome by applying a neutron flux depression correction factor /4/ which can be calculated from the transmission neutrons through the object. Unless the photon attenuation coefficient is known within the object for the different gamma-ray energies of interest, the problem is difficult to solve in the latter case. If the object however is considered to be uniformly attenuating then a mathematical correction can be applied /5/.

Experiments have been carried out in order to investigate aspects of neutron capture prompt gamma-ray emission tomography and the resulting reconstructed images are presented here.

Elsevier Sequoia S. A., Lausanne
Akadémiai Kiadó, Budapest

Theory

Consider a well collimated thermal neutron beam of flux Φ_0 which traverses an object and induces prompt gamma-rays within it (Fig. 1).

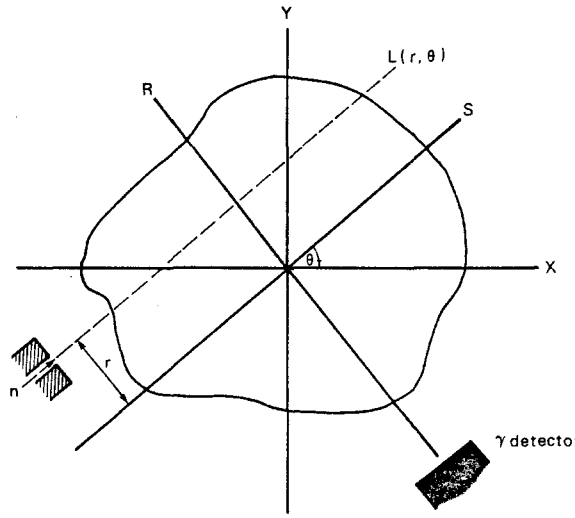

Fig. 1. Representation of the prompt gamma-ray measurement for tomography

Assuming that a narrow-beam geometry is maintained along the line $L(r,\theta)$, the number of prompt gamma-rays of interest produced along this line per unit time is given by

$$N(r,\theta) = \int_{L(r,\theta)} \frac{\Phi_0 \, Y f \, A_0 \sigma m(x,y)}{A} ds \qquad (1)$$

provided that the neutron flux does not vary along its length otherwise the flux is also a function of position. In the equation:

Y:	yield of prompt gamma-rays of interest
f:	fractional abundance of the isotope
$m(x,y)$:	mass of element at point (x,y) in the plane
A_0:	Avogadro's number
σ	microscopic capture cross-section of the nucleus
A:	atomic weight of the element of interest.

The number of gamma-rays detected is

$$D(r,\theta) = \epsilon \, N(r,\theta) t. \qquad (2)$$

where ϵ is the efficiency of the gamma-ray detector and t is the time of counting and equals the time of irradiation; or

$$D(r,\theta) = \int_{L(r,\theta)} \frac{\epsilon \, \Phi_0 \, Y \, f \, A_0 \sigma \, m(x,y) t}{A} \, ds \qquad (3)$$

and this can be written as

$$\frac{D(r,\theta) \, A}{\Phi_0 \, t \sigma \, A_0 f \, Y} = \int_{L(r,\theta)} m(x,y) \, ds \qquad (4)$$

In tomography, the reconstruction of the image is based upon solving Eq.4 for $m(x,y)$ /6/.

Experiments

Experiments were carried out employing a horizontal neutron beam ($1.8 \times 10^{12} n \; m^{-2} \; s^{-1}$), external to the high flux reactor at the Institute Laue-Langevin, Grenoble, France.

The experimental arrangement is shown in Fig.2. A neutron beam, collimated to 1 mm diameter using a 12 mm thick Li_2CO_3 plate, acted as a probe to induce prompt gamma-rays in a section of the object. Gamma-rays emitted by nuclei of interest along this probing beam were then recorded using a

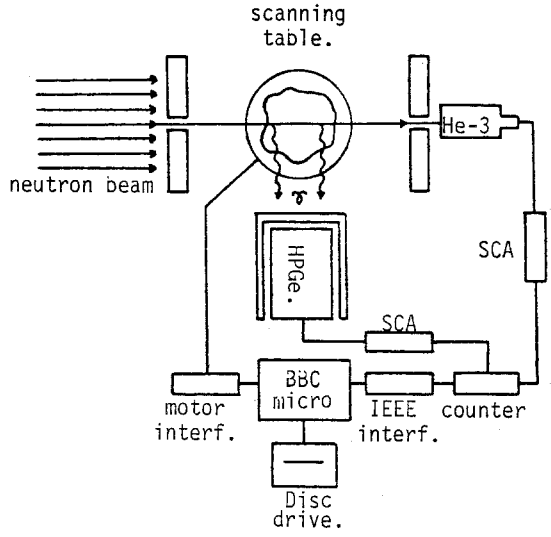

Fig.2. Experimental arrangement for measurement of transmitted neutrons and emitted prompt gamma-rays for tomography

high resolution HPGe detector positioned at 90° to the neutron beam and on the central axis of rotation of the object. The recorded gamma-rays are equivalent to the values assigned to raysums in gamma-ray emission tomography.

It is possible to measure the transmitted neutrons and emitted gamma-rays simultaneously as shown in Fig.2. The transmitted neutrons were measured using an He-3 proportional counter collimated to 1 mm diameter using 12 mm thickness of 'flexiboron'.

Two test objects were used one of lead and one of aluminium containing pellets of cadmium chloride, as shown in Fig.3.

By translating the rotating the object in front of the probing beam, a complete projection of a section through the test objects was obtained. Two energy windows were set. One at the photopeak (559 keV) prompt gamma-ray line of cadmium and the other at an energy just below, in order to estimate the contribution of the dynamic background as well as that due to scattered photons /7/ from higher energies.

The objects were scanned in order to obtain 45 projections, each comprising of 45 raysums counted for 30 second per raysum. Figure 4 shows the projections of the test objects made of Pb and Aℓ respectively, which were obtained at 0°. The three $CdCl_2$ pellets are visible and well separated.

Neutron transmission tomography of the same objects were also performed in order to obtain the distribution of the macroscopic cross-section of the objects, to be subsequently used for neutron flux depression correction. It is desirable to have both the neutron beam and the neutron detector collimated,

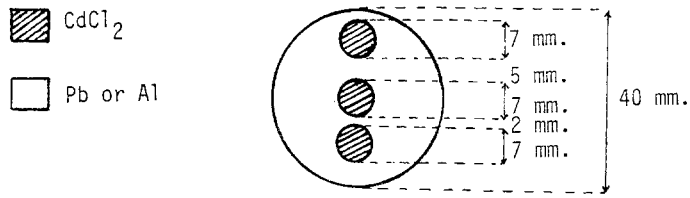

Fig.3. The cross-section of the test object

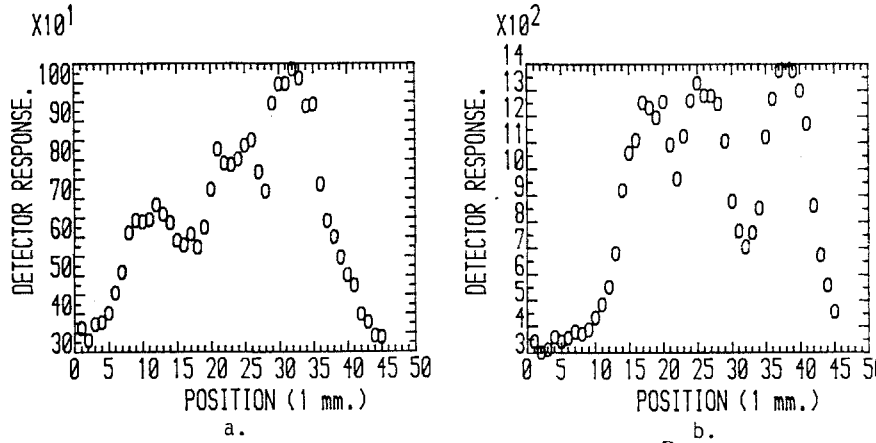

Fig.4. The projection of the test object obtained at 0°, (a) Pb matrix, (b) Aℓ matrix

but in order to overcome the problem of alignment the neutron beam was opened and the collimated neutron detector was placed as close as possible to the object to improve the solid angle subtended between the collimated detector and the object plane.

Thirty projections through 180 degrees of rotation were obtained, each comprising 61 raysums and counted for 0.1 second per raysum.

Results and discussion

The characteristics of the detecting system have been examined. The collimated neutron beam was scanned using a pellet of $CdCl_2$ of diameter 7 mm at 7, 10 and 14 mm away from the collimator and the 559 keV prompt gamma-ray peak of cadmium was recorded. The detector response against position at various distances of the pellet is shown in Fig.5.

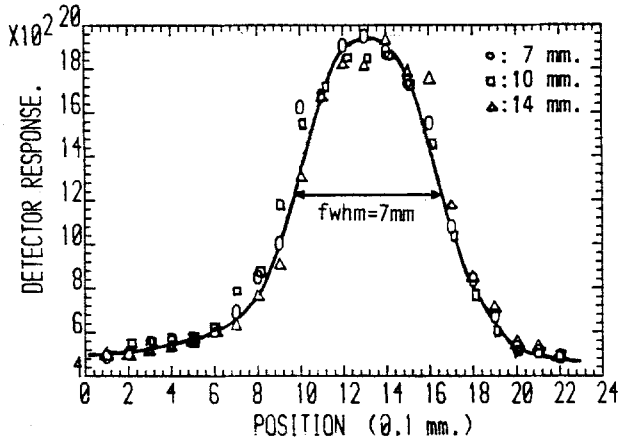

Fig.5. The line spread function of the collimated neutron beam at various positions

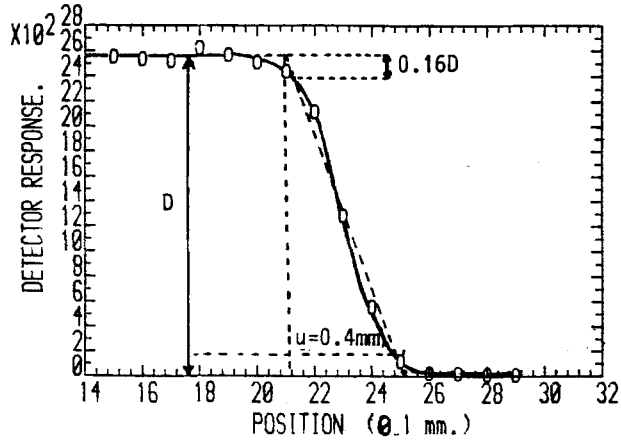

Fig.6. The step-edge spread function of the collimated He-3 detector

It can be seen from Fig.5 that the line spread function of the collimated neutron beam is the same at various distances. The full width at half maximum of these responses is found to be (7.0 ± 0.8) mm which is the diameter of the pellet. The step-edge spread function of the collimated He-3 detector shown in Fig.6 was obtained by scanning a cadmium plate, 1 mm

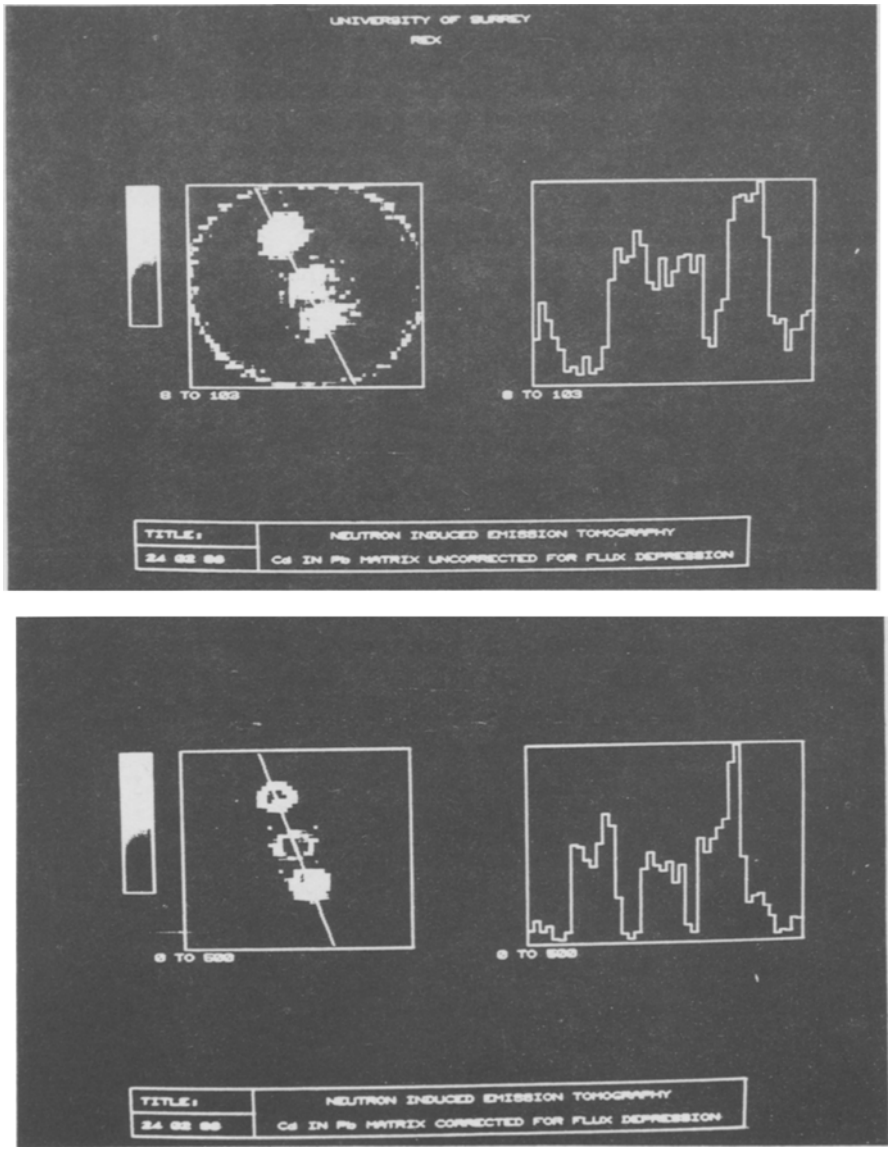

Fig.7. Reconstructed images of Cd distribution, with and without flux depression corrections, in Pb object

thickness, across the detector. The resolution or unsharpness of the system was calculated using Klasens' method /8/ and found to be (0.40 ± 0.05) mm.

The images were reconstructed using a filtered back projection algorithm and shown in Fig.7 and Fig.8 for lead and aluminium matrices, respectively. The top left hand corners are reconstructed images of the row data without any correction and the bottom left hand corners are images corrected for background and by a neutron flux depression factor. The right hand columns in Fig.7 and Fig.8 are their corresponding line scans across the images found in the left hand columns. The line scan represents the variation of the concentration of the element of interest along the line drawn. The three $CdCl_2$ pellets are not well resolved, however, when the flux depression correction is applied, these pellets can be distinguished clearly. This can also be observed in the line scan where the diameter of the pellets is found to be 7 mm and their separation by 2 mm and 5 mm (Fig.7 and Fig.8, bottom right hand corner). It was expected because of the photon attenuation that the cadmium in the aluminium

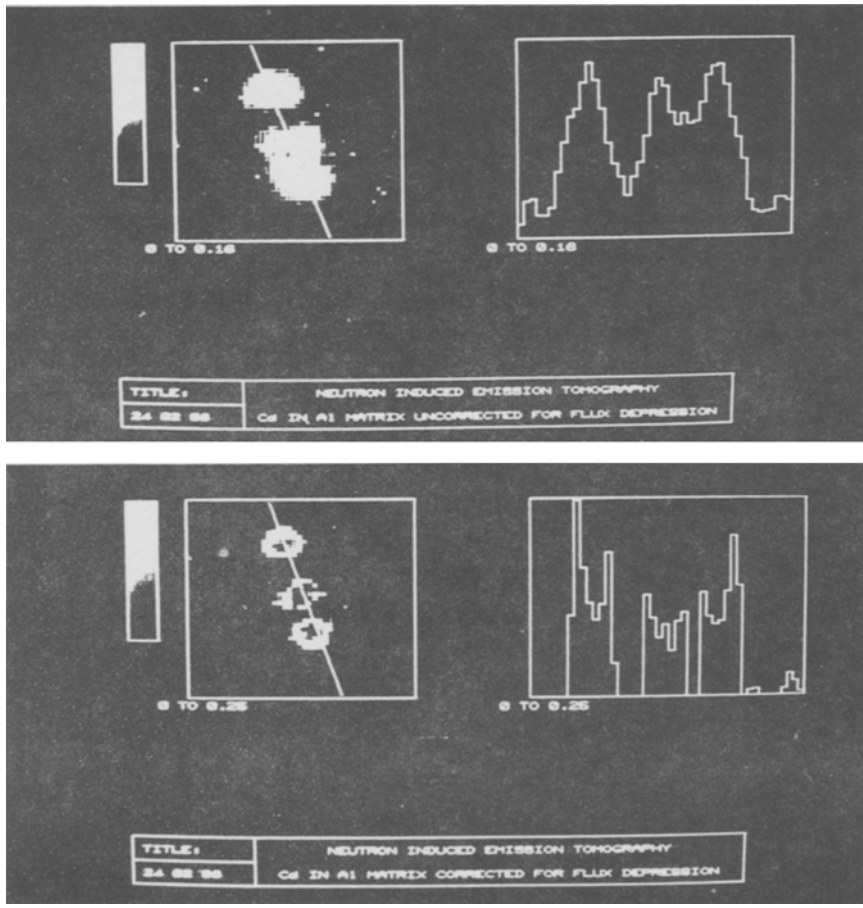

Fig.8. Reconstructed images of Cd distribution, with and without flux depression correction, in Al object

matrix will appear brighter than in the lead matrix, but the comparison can not be made since the concentration of cadmium in the pellets is not the same.

Correction due to attenuation of photons within the object was not attempted at this stage.

Conclusions

It has been shown that the three $CdCl_2$ pellets are very well resolved after correction of flux depression within the object. It suggests that flux depression or self shielding is an important consideration in this technique, especially for high cross-section material. The flux depression correction was performed raysum by raysum instead of pixel by pixel, although less accurate, because it required less computer memory and could be carried out by our BBC microcomputer (64 K).

It can be concluded from Fig. 5 that the spatial resolution of the probing beam does not vary with distance and it provides the same resolution at any point within the object thus indicating little effect due to neutron scattering.

To achieve a quantitative result, where the image exactly corresponds to elemental concentration, photon attenuation correction has to be applied and in addition the solid angle subtended by teah pixel and the gamma-ray detector has to be calculated.

In general, this study has demonstrated the feasibility of performing reconstructive tomography of the elemental distribution within the object based on the detection of neutron capture prompt gamma-rays emitted by the object, and has indicated a number of approaches along which future application can be investigated.

*

The authors would like to thank the Institute Laue-Langevin and SERC for their support. The Indonesian Government has provided a research scholarship to one of the authors (K) and (GEN) was supported by the Onassis Foundation, Greece, through a postdoctoral research grant. Thanks are also due to Dr. F. HOYLER for his help in acting as contact at the ILL.

References

1. G. DAVIES, N. M. SPYROU, I. G. HUTCHINSON, J. HUDDLESTON, Nucl. Inst. Methods, A242 (1986) 615.
2. N. M. SPYROU, Prompt and Delayed Radiation Measurements in the Elemental Analysis of Biological Materials: The case for Neutron Induced Gamma-Ray Emission Tomography, Int. Symp. on Nuclear Analytical Chemistry, June 1985. Halifax, Canada (published in J. Radional. Nucl. Chem.).
3. KUSMINARTO N. M. SPYROU, Neutron transmission tomography and neutron induced gamma-ray emission tomography, Presented at Int. Conf. on Analytical Chemistry in Nuclear Technology, June 1985, Karlsruhe, FRG.
4. N. P. BAUMAN, M. B. STROUD, Nucleonics, 23 (1965) 98.
5. T. F. BUDINGER, G. T. GULLBERG, R. H. HUESMAN, in Image Reconstruction from Projections: Implementation and Applications, G. T. HERMAN (Ed.), Springer Verlag, Berlin, 1979.
6. K. KOURIS, N. M. SPYROU, D. F. JACKSON, Imaging with Ionising Radiations, Surrey University Press/ Blackie & Son, Glasgow, I, 1982.
7. J. M. SANDERS, N. M. SPYROU, Nucl. Instr. Methods, 221 (1984) 93.
8. H. A. KLASEN, Measurement and calculation of unsharpness combinations in X-ray photography, Phys. Res. Report, 1 (1946) 4.